Pure-rotational 1D-CARS spatiotemporal thermometry with a single regenerative amplifier system

Castellanos, Leonardo; Mazza, Francesco; Kliukin, Dmitrii; Bohlin, Alexis

DOI
10.1364/OL.398982

Publication date
2020

Document Version
Final published version

Published in
Optics Letters

Optics Letters

Pure-rotational 1D-CARS spatiotemporal thermometry with a single regenerative amplifier system

Leonardo Castellanos, Francesco Mazza, Dmitrii Kliukin, and Alexis Bohlin*

Faculty of Aerospace Engineering, Delft University of Technology, Kluyverweg 1, 2629 HS Delft, The Netherlands
**Corresponding author: G.A.Bohlin@tudelft.nl*

Received 1 June 2020; revised 15 July 2020; accepted 16 July 2020; posted 20 July 2020 (Doc. ID 398982); published 18 August 2020

We report spatiotemporal pure-rotational coherent anti-Stokes Raman spectroscopy (CARS) in a one-dimensional imaging arrangement obtained with a single ultrafast regenerative amplifier system. The femtosecond pump/Stokes photon pairs, used for impulsive excitation, are delivered by an external compressor operating on a ∼35% beam split of the uncompressed amplifier output (2.5 mJ/pulse). The picosecond 1.2 mJ probe pulse is produced via the second-harmonic bandwidth compression (SHBC) of the ∼65% remainder of the amplifier output (4.5 mJ/pulse), which originates from the internal compressor. The two pump/Stokes and probe pulses are spatially, temporally, and repetition-wise correlated at the measurement, and the signal generation plane is relayed by a wide-field coherent imaging spectrometer onto the detector plane, which is refreshed at the same repetition rate as the ultrafast regenerative amplifier system. We demonstrate 1 kHz cinematographic 1D-CARS gas-phase thermometry across an unstable premixed methane/air flame-front, achieved with a single-shot precision <1% and accuracy <3%, 1.4 mm field of view, and an excellent <20 μm line-spread function.

https://doi.org/10.1364/OL.398982

Coherent anti-Stokes Raman spectroscopy (CARS) has been used to provide gas-phase quantitative scalar information (e.g., temperature and species concentration) in turbulent flows and flames for more than five decades. The technique belongs to the family of four-wave mixing, where the CARS signal is generated via the nonlinear optical interaction of three photons—denoted pump, Stokes, and probe—coupled to the internal energy states of the probed molecules. In dual-broadband pure-rotational CARS [1–3], transitions ($\Delta v = 0$, $\Delta J = \pm 2$) are induced within the entire rotational energy states manifold, and temperature is extracted from the relative intensity of the CARS spectral lines, following the Boltzmann population distribution. In hybrid femtosecond (fs)/picosecond (ps) pure-rotational CARS thermometry [4], the pump and Stokes photons are provided by broadband near-transform-limited femtosecond laser pulses, and the probe photon is provided by a narrowband picosecond laser pulse. The intra-pulse combination follows the description of simultaneous time- and frequency-resolved probing [5,6], and the excitation is termed impulsive if the duration of the femtosecond laser pulses is about one-tenth of the molecular rotational period [7] (a ∼50 fs laser pulse is required to impulsively excite N_2 with a ∼500 fs rotational period). The impulsive excitation drives the pure-rotational O- and S-branch transitions ($\Delta J = \pm 2$) with equal efficiency, which is important to maintain the thermodynamic condition of the sample. The spectral resolution of this scheme is limited by the probe pulse linewidth and, if considering the energy separation of the pure-rotational N_2 CARS spectral lines ($\Delta E_J \sim 4B = 8\ \mathrm{cm}^{-1}$), a ∼10 ps duration probe pulse would result in isolated spectral lines, dispersed at the detector. The picosecond CARS probe pulse can be efficiently produced from the broadband source using second-harmonic bandwidth compression (SHBC) [8], and is automatically repetition-wise synchronized with the pump and Stokes pulses at the measurement. The repetition rate of ultrafast regenerative amplifier laser systems is conventionally in the kHz range, and the fast sequence of pulses can be utilized for spatiotemporal CARS thermometry [9]. In addition, the high peak power of short laser pulses allows for instantaneous one- and two-dimensional pure-rotational CARS signal generation [10,11]. Single-shot CARS imaging is very powerful in the study of flame-fronts, whose propagation depends highly on spatial effects such as diffusion, mixing, and energy transfer.

In this work, we combine many of these recent advancements for pure-rotational CARS thermometry and build a new diagnostics capability with simultaneous resolution obtained in space–time, here demonstrated across an unstable premixed methane/air flame-front. In Fig. 1, the optical layout, which is based primarily on a single ultrafast regenerative amplifier system (7.5 mJ, 1 kHz, Astrella Coherent), is displayed. The laser system outputs two repetition-wise synchronized beams: the first beam is the main compressed output (∼65%, 4.5 mJ/pulse), and the second beam is an uncompressed output, which is split off before the internal compressor (∼35%, 2.5 mJ/pulse). The first beam is directed to a SHBC unit (light conversion) to produce a narrowband ∼4 ps duration probe pulse, obtained with a ∼30% conversion efficiency (1.2 mJ/pulse). The second beam is sent to an external compressor (coherent) to produce a near-transform-limited

~35 fs duration combined pump/Stokes pulse. The external compressor allows for flexible compensation (pre-chirping) of dispersion terms along the optical path, ensuring the delivery of impulsive excitation at the measurement. The path length difference between the pump/Stokes beam and the probe beam is compensated for with an optical delay line, and the relative arrival time is controlled by an automated translation stage (Thorlabs, sub-10 fs resolution). A spatial 4 f-filter, consisting of two transmission gratings (~3040 l/mm, Ibsen Photonics), two cylindrical lenses ($f := 300$ mm), and a mechanical slit, is mounted in the probe beam path to tune the probe pulse linewidth. A set of half-wave plates (Eksma Optics) is inserted to: 1) satisfy the transmission axis of the gratings (>90% diffraction efficiency at 400 nm, s-pol) for the probe beam (400 nm), 2) control the relative polarization of the pump/Stokes beam (800 nm) with respect to the probe beam, and 3) turn the polarization of the CARS beam (400 nm) to satisfy the transmission axis of the polarization beam splitter and the grating of the spectrometer. Since the spectral range of the pure-rotational N_2 CARS signal is in close vicinity of the probe beam wavelength, the probe beam needs to be rejected before the detector plane. In this work, the rejection is performed by the angle-tuning of a bandpass filter (Semrock) and is reinforced with various degrees of polarization gating [12]. The 1D-CARS signal is generated with two-beam phase matching [10], and the one-dimensional measurement geometry is formed by crossing the pump/Stokes and the probe beams, both shaped into thin sheets. The field of view (FOV) is optimized with convergent sheet-forming optics, where the irradiance of the beams is enhanced simply by compressing the laser-sheet height by shortening the CLh cylindrical lens ($f := 300$ mm at 400 nm, and $f := 1000$ mm at 800 nm) distance, relative to the CLv cylindrical lens ($f := 300$ mm at 400 nm, and $f := 500$ mm at 800 nm). The notations h-horizontal and v-vertical indicate the alignment symmetry axes of the cylindrical lenses, respectively. The FOV is limited by the ~1.4 mm height of the probe beam sheet, and the height of the pump/Stokes beam sheet is ~4 mm (fluence level ~18 TW/cm^2), as measured with a beam profiling camera (DataRay) placed at the beam crossing. The beam waists of the pump/Stokes and the probe beams are verified to be close to diffraction limited (<60 μm and <22 μm, respectively) with $M^2 = 1.2$, and the focal length of the cylindrical lenses is selected to minimize spatial averaging while retrieving the steep temperature gradient in the flame-front. The two-beam crossing angle of ~3° employed here results in a measured interaction length of ~0.6 mm; however, the requirement of spatial sectioning in the beam's longitudinal direction is relaxed at the current flame geometry. The 1D-CARS signal generation plane is relayed to the detector plane by a ~1 : 1 magnifying telescope composed of two achromatic plano-convex lenses ("spherical" SL, $f := 400$ mm). The telescope, combined with a transmission grating (~3040 l/mm, Ibsen Photonics), acts as a wide-field "slit-less" coherent imaging spectrometer. The high-dispersion grating allows for isolated spectral analysis of the pure-rotational N_2 CARS transitions, and the detection (over the range ~0 − 525 cm^{-1}, 0.25 cm^{-1}/pixel, 2048 pixels) is obtained with an instrumental broadening function (fitted with a Voigt lineshape consisting of a ~0.1 cm^{-1} FWHM Lorentzian and a ~1.8 cm^{-1} FWHM Gaussian contribution). The spatial information is retrieved with a < 20 μm FWHM line-spread function using collimating and imaging lenses with

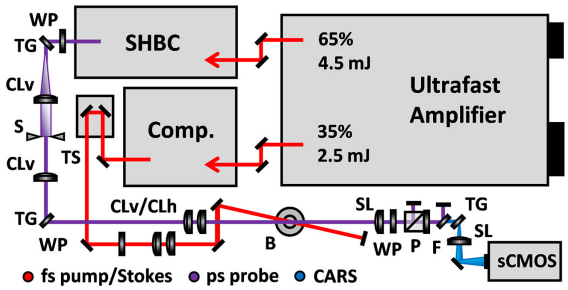

Fig. 1. Ultrafast amplifier system, combined with SHBC and an external compressor, produces auto-synchronized fs pump/Stokes and ps probe pulses for space–time 1D-CARS diagnostics. A wide-field coherent imaging spectrometer equipped with a sCMOS camera is used for fast image acquisition. TG, transmission grating; S, slit; TS, translation stage; CL, cylindrical lens with horizontal (h) and vertical (v) alignment symmetry axes; WP, half-wave plate; B, burner; P, polarizer; F, bandpass filter; SL, spherical lens.

$f := 400$ mm focal distance and 10.6 mm beam size. This was quantified by the spread of an edge response, by inserting a razor blade in the probe beam, at the CARS signal generation plane. The data rows are binned within the line-spread function ($2 \times \text{rows} = 2 \times 6.5 = 13$ μm), resulting in a digital resolution still finer than the spatial resolution. A sCMOS camera (Zyla 4.2, Andor) with manufacturer specified linearity of 99.8% and 40% quantum efficiency at 400 nm is mounted at the spectrometer image plane, allowing for repetition-wise synchronized detection, with 200 × 2048 pixel image acquisition obtained at a 1 kHz frame rate.

The SHBC technique consists of the sum-frequency generation (SFG) of phase-conjugate linearly chirped femtosecond pulses, combined in a χ_2 nonlinear crystal. A spectral filtering of the SHBC-produced probe pulse is required, because it contains both the fundamental SFG component and spectral side-bands. The spectral side-bands are due to imperfections in the conversion of the pump beams [13] and, despite being several orders of magnitude weaker than at the peak of the probe beam, their intensity is comparable to the CARS signal strength. Therefore, if not modeled correctly, the interference of these side-bands with the CARS spectral lines can obstruct the evaluation of temperature and species concentrations in the flame. We solve this by implementing a tunable pulse shaper (4 f-filter in transmission), which effectively removes the residual side-bands originating from the SFG process. As a narrow portion of the input probe pulse spectrum is transmitted through the slit of the pulse shaper, the residual temporal chirp is minimized, and the resulting pulse is near-transform-limited. The filtering occurs with minimal losses in pulse energy due to the employment of high-end transmission gratings with >90% diffraction efficiency. In Figs. 2(a) and 2(b), the temporal (13, 8, and 5 ps FWHM) and spectral (~2.7, 3.1, and 5.0 cm^{-1} FWHM) profiles of the CARS probe pulse are displayed, as resulting from different discriminating slit-widths in the pulse shaper: 70, 100, and 150 μm, respectively. Accordingly, by adjusting the opening of the mechanical slit, the probe pulse duration can easily be tuned in a wide range of 4–13 ps, with corresponding pulse energies of 1.2–0.3 mJ, respectively. The temporal profile of the probe pulse is measured through a probe-delay scan performed in argon. Argon is a noble gas, with no resonant CARS transitions. The instantaneous four-wave-mixing signal is instead a

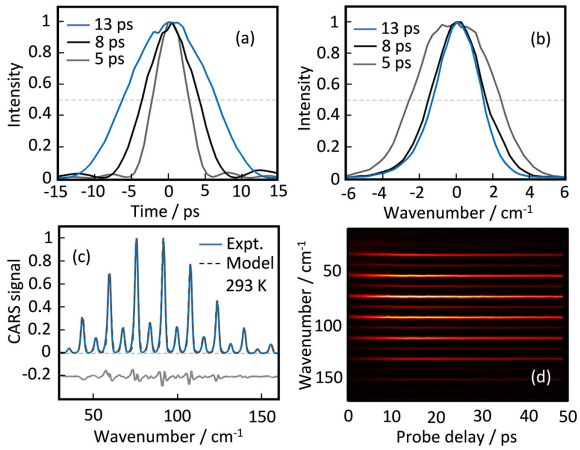

Fig. 2. Time- and frequency-domain characteristics of the SHBC-produced probe after passing through a tunable pulse shaper. (a) Temporal profile resulting in a probe pulse with a 13, 8, and 5 ps FWHM duration, respectively. (b) Corresponding bandwidths of the probe pulse are ∼2.7, 3.1, and 5 cm^{-1} FWHM. (c) Single-shot pure-rotational N_2 CARS spectrum with the best-fit of a time-domain CARS model and residuals. (d) Pure-rotational N_2 CARS spectra at variable probe delays.

non-resonant CARS signal, which is generated as a consequence of time-coinciding fs pump/Stokes and ps probe beams. Thus, a sequential delay of the beams' overlap in time (probe-delay scan), while recording the non-resonant CARS signal, maps the temporal shape of the probe pulse. The spectral profile of the probe pulse is measured with the imaging spectrometer, and after de-convolving the measured spectrum from the instrument broadening function, the results presented in Figs. 2(a) and 2(b) are in good agreement with the expected time-bandwidth product. One should be aware of the fact that the current pulse shaping, which consists of the introduction of a hard edge in the probe spectral domain, also results in slight ringing artifacts in the probe temporal profile, which is described in close analogy with the standard transform pair of a sinc function [14]. As such, the complete temporal shape of the SHBC-produced probe beam, after passing through the tunable pulse shaper, needs to be considered in the modeling of the CARS spectra. A single-shot pure-rotational N_2 CARS spectrum recorded at room temperature, with the best-fit of a time-domain CARS model (see, for instance, Refs. [4,8]) and residuals, is displayed in Fig. 2(c). Here, a ∼13 ps duration probe pulse is employed, with a ∼40 ps probe delay: the well-isolated spectral lines dispersed at the detector can be observed.

In recent works that also concern the shaping of a narrow-band picosecond probe pulse for use in fs/ps CARS (e.g., with SHBC [13,15] and volume Bragg gratings [16,17]), temporal chirp (group velocity dispersion) has been discussed as a possible artifact. Although the temporal chirp in the probe pulse can be adequately modeled for point-CARS thermometry [15], the use of a sub-10 ps probe pulse in 1D-CARS imaging becomes slightly more critical, and it is of great importance to minimize effects due to temporal chirp in the probe pulse. The presence of temporal chirp in the probe pulse has a direct impact on the CARS signal, by shifting it according to the instant central frequency of the probe pulse. This is due to the fact that the peaks in the molecular interferogram, in response to the impulsive excitation, act as a "temporal gate" on the probe pulse. Other complications, which may arise due to temporal chirp in the probe pulse, are an "uncontrolled" beating of the O_2/N_2 J-specific spectral lines and a considerable uncertainty in the spectrometer calibration. In Fig. 2(d), pure-rotational N_2 CARS spectra at variable probe delays are shown. Since the CARS signal remains at its spectral position, the absence of temporal chirp in the probe pulse with the current settings is clearly demonstrated. A spatial chirp of ∼2 cm^{-1}/mm is compensated for by floating the calibration shift of each row at the image in the spectral fitting routine.

The benchmarking of the spatiotemporal pure-rotational 1D-CARS thermometry is performed across an unstable laminar flame-front. A snap-shot photograph in Fig. 3(a) shows the used V-shaped flame, which is anchored at a steel rod (3 mm diameter) positioned ∼10 mm above a nozzle (10 mm tube diameter). The nozzle feeds the combustible mixture (premixed methane/air at $\Phi = 0.9$) with a bulk velocity of ∼1.3 m/s, controlled with rotameters (Omega) supplying the fuel- and oxidizer streams. The V-shaped laminar flame-front has a relatively flat structure and consists of a "thin" layer (∼400 μm, global thickness), where most of the exothermic reactions take place. This results in a steep temperature gradient, where almost the complete combustion history, from the unburnt mixture to the post-flame region, is covered within the ∼1.5 mm FOV.

A dataset of 1000 single-shot 1D-CARS images, each containing 200 spatially correlated spectra, was acquired at a 1 kHz frame rate. A typical single-shot 1D-CARS image is shown in Fig. 3(c). The spatial information, along the y axis, is oriented perpendicularly across the flame-front, and the x axis displays the dispersed CARS spectrum for a unique spatial position in the flame. It can be seen in Fig. 3(c) that the image is dominated by the pure-rotational N_2 CARS spectral lines (S-branch transitions), with the central weight of the spectral envelope corresponding to the local flame temperature. In addition, distinct pure-rotational O_2 CARS spectral lines can be distinguished up to the middle of the image, where most of the oxygen gets consumed in the combustion process. The CARS signal at room temperature is two orders of magnitude stronger than at flame temperature, as the signal strength scales with the square of the number density of the gas. In Fig. 3(c), the logarithm of the CARS intensity is shown, to stretch the global contrast in the image. Usually, the signal-to-background ratio rapidly degrades in the products zone, making it challenging to capture the entire temperature profile without camera saturation in the preheating zone. A balanced detection technique is employed by introducing a longer probe delay (∼40 ps), which takes advantage of the significantly higher collisional dephasing of the signal in the low temperature region of the flame. Figures 3(d) and 3(e) show single-shot CARS spectra at locations post- and pre-flame-front, respectively, which have been extracted from the CARS image in Fig. 3(c). Both spectra are background-subtracted and the spectral referencing, which accounts for the finite width of the excitation bandwidth, is performed by dividing the resonant CARS spectra with a non-resonant CARS spectrum recorded in argon. A satisfactory best-fit is obtained with a time-domain CARS model (similar to Refs. [4,8]), and is confirmed along the entire FOV. The precision and accuracy of the current CARS thermometry are evaluated in the product gases at a distance of ∼190 μm conditional to the flame-front (inferred at the 1000 K isotherm). In Fig. 3(b), the discrete probability density

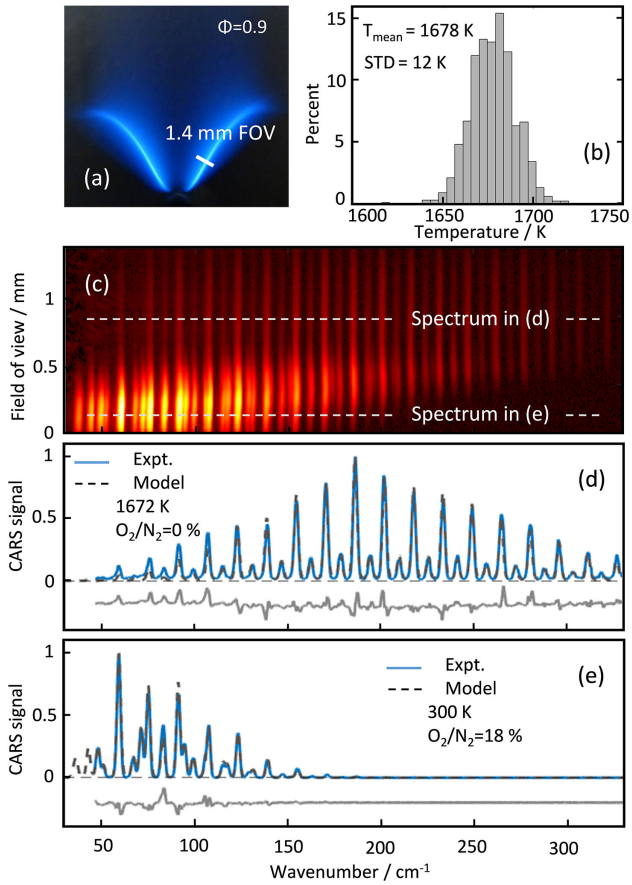

Fig. 3. (a) Snap-shot photograph of the premixed methane/air V-shaped flame-front intersected with the 1D-CARS measurement field of view. (b) Discrete probability density function from a recording in the product gases of the flame ($\Phi = 0.9$). (c) Single-shot 1D-CARS image recorded across the flame-front at 1 kHz frame rate. CARS spectrum (d) post- and (e) pre-flame-front displayed with the best-fit model and residuals.

function (PDF) obtained is reported. The CARS evaluated mean temperature $T_{mean} = 1678$ K, can be compared with an expected temperature of ~1720 K for the current flame condition as computed with the CHEM1D code [18]. A systematic deviation of ~2.5% thus results from the comparison with the numerical simulation. The main contribution to inaccuracy is ascribed to the uncertainty in the employed settings of the rotameters for controlling the oxidizer and the fuel streams. Nonetheless, the precision of the current CARS technique is ~0.7% in the central portion of the image, which has the highest excitation efficiency and probe beam intensity.

The spatiotemporal evolution of temperature and relative O_2/N_2 concentrations across the flame-front is displayed in Fig. 4. With the available space–time CARS resolution, an out-of-phase oscillating pattern with two frequencies at 13 and 75 Hz is clearly identified. We speculate that the lower frequency oscillation pattern might be caused by an unstable local equivalence ratio, induced by the volumetric flow controllers and/or buoyancy effects that provoke the formation of a Kelvin–Helmholtz-type vortex in the boundary of the flame [19]. The 75 Hz signal is most likely to be associated with internal acoustic modes of the burner.

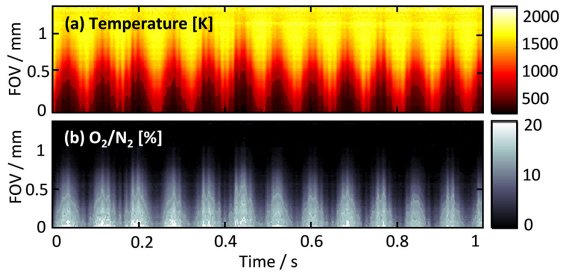

Fig. 4. Spatiotemporal evolution map of (a) temperature and (b) relative species concentration (oxygen/nitrogen) across the reaction layer of an unstable premixed flame as measured with space–time CARS resolution.

In conclusion, we have demonstrated two-beam fs/ps pure-rotational CARS line imaging at kilohertz refresh rate. This was achieved with a single regenerative amplifier system, combined with suitable compressor units, producing both the fs pump/Stokes and the ps probe beams, auto-synchronized with the detector. The current space–time CARS resolution (1.4 mm FOV and 1 kHz acquisition) allows for mapping temperature and relative species concentrations (oxygen/nitrogen) in dynamical scenes, such as those found, for instance, in moderate turbulent flames.

Funding. Netherlands Organisation for Scientific Research (VIDI grant 15690).

Disclosures. The authors declare no conflicts of interest.

REFERENCES

1. A. C. Eckbreth and T. J. Anderson, Opt. Lett. **11**, 496 (1986).
2. M. Aldén, P. E. Bengtsson, and H. Edner, Appl. Opt. **25**, 4493 (1986).
3. T. Seeger and A. Leipertz, Appl. Opt. **35**, 2665 (1996).
4. J. D. Miller, M. N. Slipchenko, T. R. Meyer, H. U. Stauffer, and J. R. Gord, Opt. Lett. **35**, 2430 (2010).
5. B. D. Prince, A. Chakraborty, B. M. Prince, and H. U. Stauffer, J. Chem. Phys. **125**, 044502 (2006).
6. D. Pestov, R. K. Murawski, G. O. Ariunbold, X. Wang, M. C. Zhi, A. V. Sokolov, V. A. Sautenkov, Y. V. Rostovtsev, A. Dogariu, Y. Huang, and M. O. Scully, Science **316**, 265 (2007).
7. N. Owschimikow, B. Schmidt, and N. Schwentner, Phys. Chem. Chem. Phys. **13**, 8671 (2011).
8. S. P. Kearney and D. J. Scoglietti, Opt. Lett. **38**, 833 (2013).
9. S. Roy, W. D. Kulatilaka, D. R. Richardson, R. P. Lucht, and J. R. Gord, Opt. Lett. **34**, 3857 (2009).
10. A. Bohlin, B. D. Patterson, and C. J. Kliewer, J. Chem. Phys. **138**, 081102 (2013).
11. A. Bohlin and C. J. Kliewer, J. Chem. Phys. **138**, 221101 (2013).
12. F. Vestin, M. Afzelius, and P.-E. Bengtsson, Proc. Combust. Inst. **31**, 833 (2007).
13. T. L. Courtney, N. T. Mecker, B. D. Patterson, M. Linne, and C. J. Kliewer, Opt. Lett. **44**, 835 (2019).
14. M. Marrocco, Opt. Lett. **39**, 4831 (2014).
15. C. Yang, D. Escofet-Martin, D. Dunn-Rankin, Y. C. Chien, X. Yu, and S. Mukamel, J. Raman Spectrosc. **48**, 1881 (2017).
16. R. Santagata, M. Scherman, M. Toubeix, M. Nafa, B. Tretout, and A. Bresson, Opt. Express **27**, 32924 (2019).
17. K. Arafat Rahman, E. L. Braun, M. N. Slipchenko, S. Roy, and T. R. Meyer, Opt. Lett. **45**, 503 (2020).
18. J. A. van Oijen and P. de Goey, Combust. Sci. Technol. **161**, 113 (2000).
19. A. I. Krikunova, Phys. Fluids **31**, 123607 (2019).